Forward-scattered light: Spectral broadening and temporal coherence

N. L. Swanson
Coastal Systems Station, Naval Surface Warfare Center, Dahlgren Division, Panama City, Florida 32407

D. H. Van Winkle
Department of Physics, Center for Materials Research and Technology, Florida State University, Tallahassee, Florida 32306

(Received 4 December 1995; revised manuscript received 23 September 1996)

Fabry-Pérot spectroscopy was used to observe a spectral broadening of 1.3 ± 0.2 MHz in laser light forward scattered through a colloidal solution. Light from a single-mode argon-ion laser was collected after scattering through water to which measured amounts of diatomaceous earth or 0.08-μm-diam polystyrene spheres were successively added. The broadening is attributed to coupling between fluctuations in particle concentration and spontaneous thermal fluctuations. Though spontaneous fluctuations exist in all pure fluids, they are very weak in water. However, the presence of the particles induces temperature gradients in the fluid, which in turn induce fluctuations in particle concentration. [S1050-2947(97)03906-1]

PACS number(s): 42.55.−f

I. INTRODUCTION

Through a series of serendipitous coincidences, a spectral broadening of light forward scattered through colloidal solutions was discovered. For several years, it has been known that laser radiation in an ambient light background can be detected using interferometric techniques to distinguish the light by its coherence length [1]. It was proposed that a related interferometric technique might be useful to distinguish between laser light that has been scattered and that which has not been scattered. The suggestion was that the characteristic frequency of the scattered light would be broadened by energy exchange with the surrounding medium. If an interferometer could be set to reject the broadened frequencies and retain the unscattered light, then the image thus formed would be composed of only unscattered light. Upon measuring the spectra of 514.5-nm laser light forward scattered through water as a function of added colloidal particles (typically polystyrene spheres or diatomaceous earth) it was found that in some cases the unscattered 1.5-MHz linewidth was broadened by a factor of 2.

Light-scattering experiments involving colloidal particles are typically considered quasielastic experiments. The dominant scattering signal is from the index of refraction fluctuations, which do not change the magnitude of the light's wave vector, but do change the direction. Inelastic-scattering experiments involve the creation or annihilation of phonons in the medium. High-energy phonons (optical modes in semiconductors, vibrational or rotational modes in molecules) are studied by Raman scattering. We did not study Raman scattering in our system. Lower-energy phonons (acoustic modes in semiconductors or propagating density waves in fluids) are studied by Brilluoin scattering. The two Brillouin peaks are centered at $\omega=ck\pm c_s k$, where c is the speed of light, k is the wave number of the laser, and c_s is the adiabatic sound velocity in the fluid. In addition to Brillouin peaks, the Rayleigh peak is centered at $\omega_0=ck$. The Rayleigh mode is associated with diffusive thermal relaxations [2–4].

In typical Rayleigh scattering experiments, the broadening of the Rayleigh peak upon scattering from a single species is observed at a scattering angle of 90° relative to the transmitted beam. In those systems it is clear that all collected light is scattered. For forward-scattered light, where the scattering angle $\theta\cong0$, the collected light may or may not have been scattered. The magnitude of the frequency shift is proportional to $\sin^2(\theta/2)$. Thus Rayleigh scattering theory predicts zero broadening in the frequency spectrum for forward-scattered light.

The relative intensity of the Rayleigh peak to the Brillouin peaks is proportional to $1-c_v/c_p$. In water $c_p\approx c_v$; therefore the broadening of the central peak due to scattering from thermal fluctuations is expected to be very weak [5,6]. The width of the Rayleigh scattered light has been shown [7,8] to be proportional to $\kappa/\rho_0 c_p$, where κ is the thermal conductivity, ρ_0 is the equilibrium number density, and c_p is the specific heat at constant pressure of the fluid. This broadening in pure fluids is essentially associated with temperature fluctuations at constant pressure and their associated diffusive damping.

With the addition of particles, the system becomes significantly more complex. By relating the theory of scattering from binary fluid mixtures to our observations, we are able to understand the broadening observed as being due to local fluctuations in particle concentration coupling to fluctuations in the thermal phonon distribution in the fluid. Much work has been done using quasielastic light-scattering spectroscopy (QELSS) to measure diffusional broadening due to the collective fluctuations of colloidal polystyrene spheres in aqueous solutions [7,9]. Though new correlators can respond fast enough, QELSS generally probes much slower processes than are measured in this experiment. Recently, the theory for the spectral broadening associated with particle diffusion coupling to the transverse viscous modes in externally driven systems was developed by Schmitz [10]. The calculated contribution of the viscous modes to the diffusional broadening is similar in magnitude to the diffusional broadening itself. Both are well below the resolution of the Fabry-Pérot spectrometer used in our experiment. Also, nonequilibrium fluctuations induced by applying a temperature gradient to a sample have been shown to result in the viscous modes coupling to the thermal modes [11]. The broadening associated with these viscous modes is similar in magnitude to the ther-

mal fluctuation broadening. The relative intensity is proportional to the temperature difference across the sample. The measurements reported here do not have a viscous mode component since thermal gradients were insignificant.

In order to further understand the measured broadening, we quantitatively examine the associated loss in coherence length. In this paper we first outline the relationship between the spectrum of a light source and its coherence length. Next we present an outline of the theory of scattering from binary fluid mixtures. We then describe the experimental procedure and analyze the data approximating the colloidal-water mixture as a binary fluid. A scattered spectrum was generated from the theoretical calculations and compared with the measured scattered spectrum.

II. THEORY

The coherence properties of a beam can be determined from the correlation functions of the electric fields. Spatial coherence is expressed in terms of the cross-correlation function $\langle E_1^*(t)E_2(t+\tau)\rangle$, where E_1 is the field measured at a point P_1 and E_2 is the field measured at point P_2 in the wave field. Temporal coherence is determined from the autocorrelation function

$$\Gamma(\tau)=\langle E_1^*(t)E_1(t+\tau)\rangle. \tag{1}$$

The normalized *degree of coherence* is defined as

$$\gamma(\tau)=\frac{\Gamma(\tau)}{\Gamma(0)}=\frac{\langle E^*(t)E(t+\tau)\rangle}{\langle|E(t)|^2\rangle}. \tag{2}$$

The coherence time is defined [12] in terms of the degree of coherence

$$\tau_c=\int_{-\infty}^{\infty}|\gamma(\tau)|^2 d\tau. \tag{3}$$

The coherence length is then $l_c=c\tau_c$. The power spectrum $I(\omega)$ is the Fourier transform of the correlation function $\Gamma(\tau)$. By measuring the power spectrum, the degree of coherence $\gamma(\tau)$ can be obtained directly in a single measurement because

$$\Gamma(\tau)=\frac{1}{\sqrt{2\pi}}\int_{-\infty}^{\infty}e^{i\omega\tau}I(\omega)d\omega. \tag{4}$$

In the Rayleigh scattering model, it can be shown [13] that the scattered spectrum is given by

$$I(\omega)=N\,\frac{\alpha^2|E_0|^2\omega_0^4\cos^2\theta_s}{c^4R^2}\,S(\omega), \tag{5}$$

where $S(\omega)$ is the structure function, N is the number of particles in the scattering volume, α is the particle polarizability, E_0 is the incident field, ω_0 is the frequency of the incident field, θ_s is the scattering angle, c is the speed of light, and R is the distance from the scattering volume to the point of observation. The assumptions used in this model are that R is much larger than the dimensions of the scattering volume, the light is plane polarized, the particle size is much smaller than the wavelength, the particles are identical, and there are single-scattering events only. The restriction on the particle size arises from the use of the dipole approximation [13,14] in the calculation of the scattered field. If the structure function governing the scattering is known, the power spectrum can be calculated from Eq. (5).

The extinction of a laser beam traversing an optical path in water can be described by

$$I(z)=I_0e^{-\xi z}, \tag{6}$$

where $I(z)$ is the intensity at z, I_0 is the intensity at $z=0$, and ξ is the extinction coefficient, also called the beam attenuation coefficient. The extinction coefficient is equal to the absorption coefficient plus the scattering coefficient, i.e., $\xi=a+s$. It is therefore a measure of the number and type of particles present in the water. Since polystyrene spheres and diatomaceous earth do not absorb at optical frequencies, we assume that $\xi\cong s$. The product ξz, which we will designate as the *optical density* (OD), is the appropriate dependent variable for expressing the relative increase in scattering as particles are added to the water. Equation (6) is sometimes written $I=I_0 10^{\xi_{10}z}$, where $\xi_{10}=\xi\log_{10}e$. In this case the optical density is the product $\xi_{10}z$. The attenuation measured in this way is more common to describe optical properties of filters.

Data were taken as colloidal particles were successively added to clear water. Very few scattering events occur in clear water; therefore the assumption of single scattering required for applying the Rayleigh model is appropriate for low optical densities. As the OD ($D_{\rm opt}$) increases the single-scattering assumption will break down. It is necessary to determine the range of the applicability of the single-scattering theory.

It is postulated that the transition to significant multiple scattering occurs when $D_{\rm opt}\cong 1$. The mean free path of the photon is given by

$$l_{\rm mfp}=\frac{1}{\rho\sigma}, \tag{7}$$

where ρ is the particle density and σ is the scattering cross section. According to the *optical theorem* [15], the seattering cross section is

$$\sigma=\frac{\xi}{\rho}. \tag{8}$$

The mean free path is thus $l_{\rm mfp}=1/\xi$. As particles are added to the water the mean free path, $l_{\rm mfp}$ decreases. When $D_{\rm opt}=\xi z=1$, $l_{\rm mfp}$ is equal to z, the optical path length. We therefore postulate that if $D_{\rm opt}<1$, the scattered light will have been scattered only once. When $D_{\rm opt}>1$ multiple-scattering events will become more significant. Therefore, the single-scattering assumption will break down when $D_{\rm opt}>1$.

Normally colloidal solutions are described in terms of particle diffusion. Pure water systems are described in terms of thermal fluctuations. When the particles achieve high enough density to interact with the thermal fluctuations in the fluid, both descriptions break down. As a first step to understanding this physical system we assume the particle-water solution is similar to a binary fluid.

In a binary fluid mixture the two components interact in a complicated way. In a pure fluid there exist spontaneous fluctuations in temperature and density at the microscopic level. These fluctuations can be created and annihilated upon interaction with photons during scattering processes. Accord-

ing to the Onsager regression hypothesis [9], the spontaneous fluctuations regress to equilibrium according to the same relaxation equations that describe the macroscopic relaxation processes. It is therefore appropriate to describe this process by the hydrodynamic equations, i.e., the continuity equation, the Navier-Stokes equation, and the energy transport equation. This is a set of nonlinear, partial differential equations. The full treatment for a binary mixture requires solving these three equations plus the diffusion equation describing concentration fluctuations for a two-component fluid [16]. The equations are linearized by assuming small fluctuations about equilibrium in the thermodynamic variables (pressure, density, temperature, momentum, entropy, and concentration) and retaining only first-order fluctuation terms. For our analysis the shifted Brillouin peaks are not of interest. We therefore assume a uniform pressure so that the fluctuations in pressure and velocity vanish from the equations. This is a special case of no sound modes and therefore no Brillouin doublets. The continuity equation and the longitudinal Navier-Stokes equation become trivial. Following the development by Berne and Pecora [9], the linearized diffusion and energy transport equations are then functions of only the concentration and thermal fluctuations,

$$\frac{\partial c'}{\partial t}=D\left\{\nabla^2 c'+\frac{K_T}{T_0}\nabla^2 T'\right\},$$
$$\frac{\partial T'}{\partial t}-\frac{K_T}{c_p}\left(\frac{\partial \mu}{\partial c}\right)_{p,T}\frac{\partial c'}{\partial t}=\chi\nabla^2 T', \tag{9}$$

where the concentration fluctuation $c'=\delta c(\vec{r},t)$ and the temperature fluctuation $T'=\delta T(\vec{r},t)$ are the first-order perturbations about the equilibrium values c_0 and T_0. The remaining terms in Eq. (9) are as follows: $K_T\equiv c_1 c_3(x/D)$ is the thermal diffusion ratio, T is the temperature, μ is the chemical potential of the mixture, D is the mutual diffusion coefficient of the two components, χ is the thermal diffusivity, c_1 and c_2 are the concentrations of two components, and c_p is the specific heat of the mixture at constant pressure. When c appears without a subscript, it represents the concentration of component 1. The concentration is defined as $c_1=M_1/M$, where $M=M_1+M_2$ is the total mass of the mixture.

Taking the Fourier-Laplace transform of Eq. (9) gives

$$(s+q^2D)\tilde{c}'(\vec{q},s)+q^2\left(\frac{K_T D}{T_0}\right)\tilde{T}'(\vec{q},s)=c'(\vec{q},0),$$
$$-s\left(\frac{K_T}{c_p}\right)\left(\frac{\partial \mu}{\partial c}\right)_{p,T}\tilde{c}'(\vec{q},s)+(s+\chi q^2)\tilde{T}'(\vec{q},s)$$
$$=\tilde{T}'(\vec{q},0)-\frac{K_T}{c_p}\left(\frac{\partial \mu}{\partial c}\right)_{p,T}c'(\vec{q},0), \tag{10}$$

where **q** is the scattering vector. This set of linear equations is solved by matrix methods to obtain

$$\begin{pmatrix}\tilde{c}'(\vec{q},s)\\ \tilde{T}'(\vec{q},s)\end{pmatrix}=\frac{1}{\det(M)}\begin{pmatrix}(s+\chi q^2)+q^2\left(\frac{K_T^2 D}{c_p T_0}\right)\left(\frac{\partial \mu}{\partial c}\right)_{p,T} & -q^2\left(\frac{K_T D}{T_0}\right)\\ -q^2\left(\frac{K_T D}{c_p}\right)\left(\frac{\partial \mu}{\partial c}\right)_{p,T} & s+Dq^2\end{pmatrix}\begin{pmatrix}c'(\vec{q},0)\\ T'(\vec{q},0)\end{pmatrix}, \tag{11}$$

where M is the initial matrix given by

$$M=\begin{pmatrix}s+q^2D & q^2\left(\frac{K_T D}{T_0}\right)\\ -s\left(\frac{K_T}{c_p}\right)\left(\frac{\partial \mu}{\partial c}\right)_{p,T} & s+q^2\chi\end{pmatrix}. \tag{12}$$

The structure function is given by

$$S(\vec{q},\omega)=\int e^{-i\omega t}\langle \delta\varepsilon^*(\vec{q},0)\,\delta\varepsilon(\vec{q},t)\rangle dt, \tag{13}$$

where $\delta\varepsilon$ is the fluctuation in the dielectric constant. By explicitly writing the solutions for $\tilde{c}'(\vec{q},s)$ and $\tilde{T}'(\vec{q},s)$ and taking the inverse Laplace transform, the fluctuation in the dielectric constant can be written in terms of the concentration and temperature fluctuations

$$\delta\varepsilon(\vec{q},t)=\left(\frac{\partial \varepsilon}{\partial c}\right)_{p,T}c'(\vec{q},t)+\left(\frac{\partial \varepsilon}{\partial T}\right)_{p,c}T'(\vec{q},t). \tag{14}$$

Substituting the concentration and thermal fluctuations from Eq. (11) into Eq. (14) and taking the Fourier transform in Eq. (13) yields the structure function

$$S(q,\omega)=\frac{2k_BT}{z_--z_+}\left(\frac{\partial\varepsilon}{\partial c}\right)^2_{p,T}\left(\frac{\partial c}{\partial\mu}\right)_{p,T}\left\{\frac{(z_--Dq^2)z_+}{\omega^2+z_+^2}-\frac{(z_+-Dq^2)z_-}{\omega^2+z_-^2}\right\}+2\left(\frac{\partial\varepsilon}{\partial c}\right)_{p,T}\left(\frac{\partial\varepsilon}{\partial T}\right)_{p,c}\times\frac{K_TDq^2}{c_p\rho V}\left\{\frac{z_-}{\omega^2+z_-^2}-\frac{z_+}{\omega^2+z_+^2}\right\}+\left(\frac{\partial\varepsilon}{\partial T}\right)^2_{p,c}\times\frac{T}{c_p\rho V}\left\{\frac{(Dq^2-z_+)z_+}{\omega^2+z_+^2}-\frac{(Dq^2-z_-)z_-}{\omega^2+z_-^2}\right\},\tag{15}$$

from which the power spectrum and correlation function may be calculated. The spectrum is the superposition of two Lorentzian bands

$$\frac{z_+}{\omega^2+z_+^2},\quad \frac{z_-}{\omega^2+z_-^2},$$

where

$$z_\pm=\frac{q^2}{2}\left[\left\{\chi+D\left[1+\frac{k_T^2}{Tc_p}\left(\frac{\partial\mu}{\partial c}\right)_{p,T}\right]\right\}\pm\left(\left\{\chi+D\left[1+\frac{k_T^2}{Tc_p}\left(\frac{\partial\mu}{\partial c}\right)_{p,T}\right]\right\}-4\chi D\right)^{1/2}\right].\tag{16}$$

The particle diffusion spectrum (associated with D) and the entropy fluctuation spectrum (associated with χ) are coupled in a complicated way. In nonequilibrium thermodynamics this coupling is known as the Dufour effect (concentration gradient inducing heat flow) and the Soret effect (temperature gradient inducing diffusion flux) [17].

To introduce the analogy, we propose that the particles comprise component 1 above. The mutual diffusion coefficient D expresses the coupled diffusion of the two components. The concentration of particles is small and the particles are much larger than the fluid molecules, thus D reduces to the particle diffusion coefficient. For most liquids it is usually the case that the thermal diffusivity, given by

$$\chi=\frac{\kappa}{\rho c_p},\tag{17}$$

where ρ is the fluid density, is much greater than the particle diffusion D. For water, $\chi=0.0214$ cm^2/s. The particle diffusion coefficient is

$$D=\frac{k_BT}{6\pi\eta r},\tag{18}$$

where η is the sheer viscosity of the fluid and r is the radius of the particles. For the 0.08-μm spheres $D=5.35\times10^{-8}$ cm^2/s. Values for the constants were obtained from the CRC handbook [23]. Thus the limit $\chi\gg D$ is satisfied, in which case

$$z_+\to\chi q^2,\quad z_-\to Dq^2.\tag{19}$$

The structure function in Eq. (15) then simplifies to

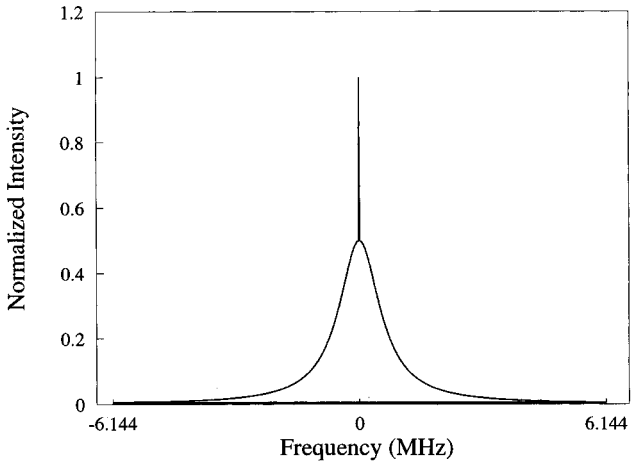

FIG. 1. Power spectrum for scattering from a binary fluid with equal parts particle and thermal diffusion.

$$S(k,\omega)\approx\left\{A\,\frac{Dq^2}{\omega^2+(Dq^2)^2}+B\,\frac{\chi q^2}{\omega^2+(\chi q^2)^2}\right\},\tag{20}$$

where

$$A=2k_BT\left(\frac{\partial\varepsilon}{\partial c}\right)_{p,T}\left[\left(\frac{\partial\varepsilon}{\partial c}\right)_{p,T}\left(\frac{\partial c}{\partial\mu}\right)_{p,T}-2\left(\frac{\partial\varepsilon}{\partial T}\right)_{p,c}\frac{c_1c_2}{c_p\rho V}\right],\tag{21}$$

$$B=\frac{2k_BT}{c_p\rho V}\left(\frac{\partial\varepsilon}{\partial T}\right)_{p,c}\left[T\left(\frac{\partial\varepsilon}{\partial T}\right)_{p,c}+2\left(\frac{\partial\varepsilon}{\partial c}\right)_{p,T}c_1c_2\right].$$

When there are no particles present in the mixture $c_1\to0$, in which case $A=0$ and the second term on the right-hand side of the equation for B also goes to zero. Then Eq. (20) reduces to the structure function for the thermal fluctuations in a pure fluid.

The spectrum in Eq. (20) is the sum of two Lorentzian spectra, one due to particle diffusion and the other to thermal diffusion. The fluctuation in the dielectric constant with respect to fluctuations in concentration can be related to fluctuations in the refractive index of the mixture. Information on the derivatives in Eq. (21) for water-diatomaceous earth or water-polystyrene mixtures was unavailable. For illustrative purposes, we assume $A=B=0.5$ and $\theta=0.08$ rad. That is, the particle diffusion and the thermal fluctuations contribute equally to the scattered spectrum. The structure function in Eq. (20) was calculated for these values and the result is graphed in Fig. 1. The particle diffusion component is a sharp, narrow peak sitting on top of a much broader peak arising from thermal diffusivity.

III. EXPERIMENT

Experiments were carried out using an argon-ion laser operating at 40 mW. Incorporated in this laser is an additional etalon resulting in a single-mode spectral output with a width of approximately 0.5 MHz. In all experiments the

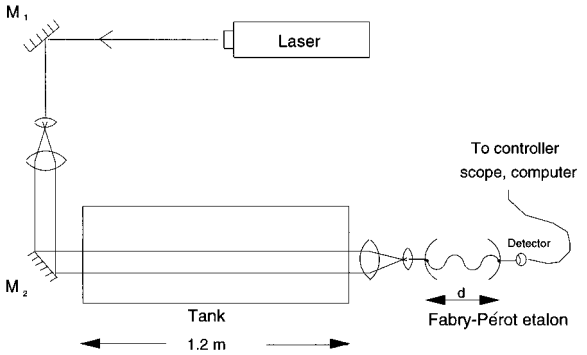

FIG. 2. Experimental setup.

514.5-nm green line was used. Figure 2 shows the basic experimental setup. The beam was expanded and passed through a 5.5-cm aperture. After the light passed through the tank, it was collected with an inverse beam expander (telescope) and input to a Fabry-Pérot spectrometer [18]. The collection lens was 10 cm in diameter. The pinhole (spatial filter) was removed from the inverse telescope because it would have blocked the scattered light.

The dimensions of the tank were $1.21\times0.31\times0.74$ m^3. For each experiment, the tank was initially filled with tap water filtered and deionized (18 MΩ) by a filtration system with an additional 0.2-μm filter at the output. Successive spectral data were taken between adding measured amounts of either diatomaceous earth or polystyrene spheres to the water. Because the density of diatomaceous earth is greater than the density of water, magnetic stirrers were used to keep the particles in suspension. The magnets were 7.62 cm in length, rotating at 90 rpm inside the tank.

The optical path length was fixed by the length of the tank $L=1.21$ m. The properties of the beam attenuation coefficient ξ depend on the number and type of suspended particles in the water and the wavelength of the light. The product ξL, which we have defined as the OD, is a dimensionless quantity that gives the overall extinction of the beam. All data were taken as a function of the OD by simultaneously measuring the beam attenuation coefficient ξ with a transmissometer operating at 510 nm.

The bandwidth of the Fabry-Pérot spectrometer was measured at 514 nm and found to be 1.38 MHz. The *free spectral range* was 300 MHz. The output of the spectrometer was detected by a photodiode and the signal from the photodiode fed to a controller. The controller provides a ramped high voltage signal to the piezoelectric crystal for scanning the spectrum. It also amplifies the signal from the photodiode and provides a trigger for display on an oscilloscope. The signal from the controller was then input to an oscilloscope and the digitized trace was transferred to a portable computer via a GPIB-IEEE interface. Thirty-one spectral traces were recorded for each concentration of colloidal particles. The spectra shown in all of the figures represent the average of the 31 traces.

Broadening was initially observed in a sample where diatomaceous earth was incrementally added to the water. Diatomaceous earth is composed of diatoms and fragments encompassing a large range of shapes and sizes (10 nm–10 μm). The experiment was repeated using polystyrene spheres of diameters 0.08, 0.54, and 5.17 μm. These sizes were chosen because they are less than, approximately equal to, and greater than the 0.514-μm wavelength of the laser. The asymmetric shape of the diatomaceous earth particles can cause a depolarized broadening in the central Rayleigh peak due to orientational relaxation [19,20]. Broadening due to orientational relaxation can also occur for materials that exhibit intrinsic optical anisotropy, e.g., uniaxial materials. With the spherically symmetric particles, any measured broadening would rule out this anisotropic broadening.

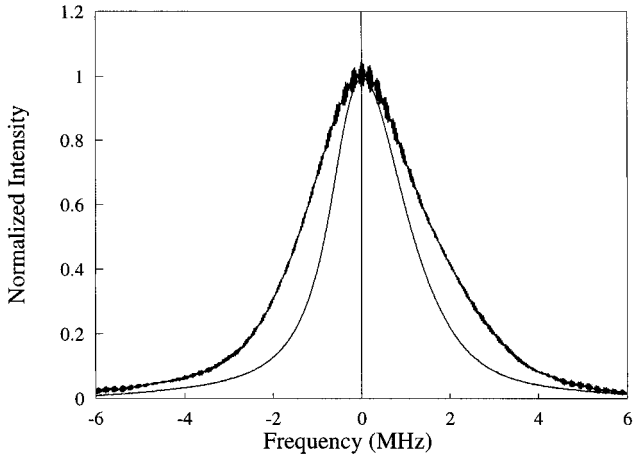

FIG. 3. Power spectra of the laser through clear water and water plus 0.08-μm spheres. The narrow spectrum is the measurement through clear water and the broadened spectrum was measured through water with spheres added.

We observed no change in the measured spectra for experiments performed using the two larger sizes of spheres. Only the smallest 0.08-μm spheres exhibited any measurable change in bandwidth. The results for the diatomaceous earth and the 0.08-μm spheres were nearly identical. Plots of the scattered spectra for the 0.08-μm spheres are shown in Fig. 3. The narrow spectrum is the laser in clear water at $D_{\rm opt}=0.048$. It has a width of 2.06 MHz. The broadened spectrum was taken of the laser scattered through water $+4.6$ ml of spheres at 8.4% solids (2.69×10^{14} spheres/ml). The measured $D_{\rm opt}=1.07$ and the width is 3.46 MHz for a change of 1.40 MHz. The change in the bandwidth for the diatomaceous earth experiment is 1.23 MHz.

The spectra have been normalized for comparison. The actual intensity of the spectrum measured through very turbid water was orders of magnitude less than that measured through clear water. We believe the apparent substructure in the spectra measured through turbid water is due to added electronic noise when the gain is increased. The substructure has a frequency of approximately 0.2 MHz, which is far below the resolution of the instrument. Furthermore, the flat trace when the beam was blocked also had this 0.5-MHz noise at high gain.

The coherence length was calculated and plotted against the OD as shown in Fig. 4. The coherence length starts at 68 m and drops to $\sim$52 m. There does not appear to be any additional drop in the coherence length as particles are further added to the mixture beyond $D_{\rm opt}\approx1$. Since the results for the diatomaceous earth and the 0.08-μm spheres were statistically indistinguishable, any contributions to the broadening from rotational effects can be eliminated. Thus the

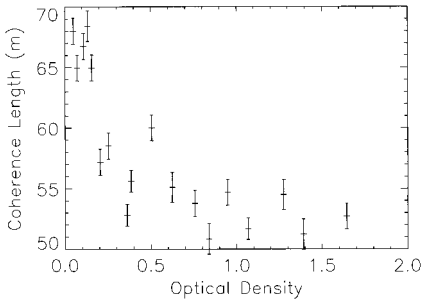

FIG. 4. Coherence length vs optical density for measurements taken through water with 0.08-μm spheres added.

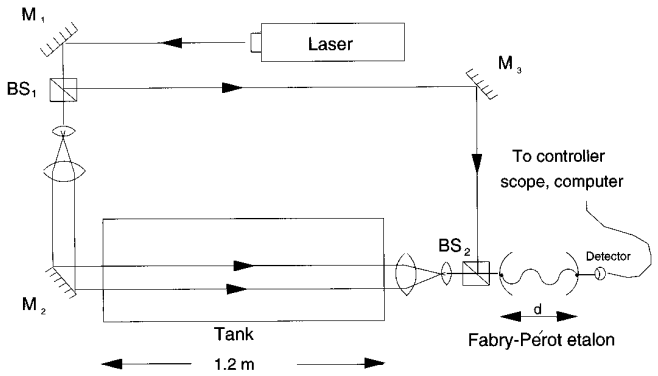

FIG. 5. Experimental setup for simultaneously measuring the power spectra of the laser through air and through water with diatomaceous earth added.

Rayleigh model is appropriate to describe the scattering since spectral broadening was observed only when the particles were smaller than the wavelength of the laser.

The error in l_c was obtained from the standard deviation of the mean for 31 measurements. The calculated value of l_c, based on the measured spectrum, is substantially affected by the spectrometer's instrumental bandwidth. It is therefore not an absolute measurement of the coherence length of the laser. Only the change in l_c is of interest. The spectral profile for a resonant cavity (both the laser and the Fabry-Pérot étalon) is dependent on the reflectivity, parallelism, and flatness of the mirrors [21]. It is usually a Voigt function, i.e., the convolution of a Gaussian function with a Lorentzian function. Further, the measured signal is the convolution of the laser spectrum with the instrument response function. The ideal situation is when the width of the laser spectrum is much greater than the width of the spectrometer response function. The spectrometer response can then be considered a δ function (by comparison) and the convolution (measurement) returns the spectral profile of the laser. This was not the case in these experiments and as a result the spectrometer is operating very near its limits causing fluctuations in the spectral traces. This is why 31 traces were recorded and averaged for each measurement. The error in the OD is the transmissometer instrumental error $\pm 5\%$. Systematic errors in the value of the OD may result from imperfect mixing of the diatomaceous earth and thus the actual OD may be smaller or larger than the average measured by the transmissometer.

It should be noted that the spectrometer must be realigned between measurements taken in air and with water in the tank. Adding water to the tank causes a lateral offset in the collected beam if the tank is not perfectly perpendicular to the beam. This causes misalignment of the spectrometer. Theoretically, this could be compensated. However, since the laser spectrum is narrow compared to the instrument response function, the alignment is critical. A minute misalignment can lead to different results, especially when trying to fit the spectra to Lorentzian, Gaussian, or Voigt functions. This makes it impossible to directly compare the spectra of the laser measured in air with those measured through water. The spectrum for the beam passing through the empty tank (laser in air) was nearly identical to that for clear water. For these reasons, the spectrum measured through turbid water is compared with the measurement made through clear, filtered water and not air.

Since the measured broadening is small and all measurements are taken very close to the limits of the Fabry-Pérot spectrometer, we decided to set up an experiment repeating the measurements of the spectra through water and diatomaceous earth while simultaneously taking measurements of the laser in air. This ensures that the broadening effect is real and not a consequence of changes in the Fabry-Pérot over time (e.g., temperature). Figure 5 is a diagram of the experimental setup. The beam is split at the first beam splitter BS1 and recombined at BS2. The tank was filled with filtered water. The beam in air was blocked, while the first measurement was taken in clear water. The beam from the tank was then blocked and a measurement was taken of the laser in air. This process was repeated as particles were added to the water throughout the entire experiment. Every time a measurement was taken of the laser through the water mixture, a subsequent measurement of the laser in air was also taken.

Results of this confirming experiment are shown in Fig. 6. It is clear from these data that the coherence length of the laser in air does not change, while l_c through the water mixture changes as before. The coherence length for the laser in air *appears* to be less than that through water. This is because the two beams were not perfectly coaxial and the alignment was much better for the beam passing through the tank than for the beam through air. This also illustrates how crucial the alignment is to the experimental results.

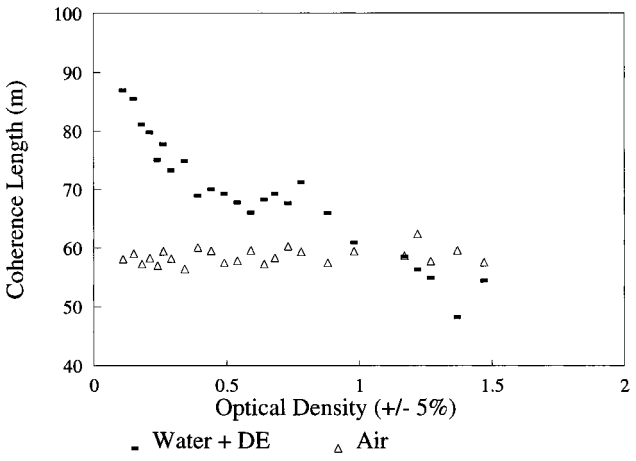

FIG. 6. Coherence length vs optical density for simultaneous measurement of the laser through water with diatomaceous earth (DE) and the laser through air.

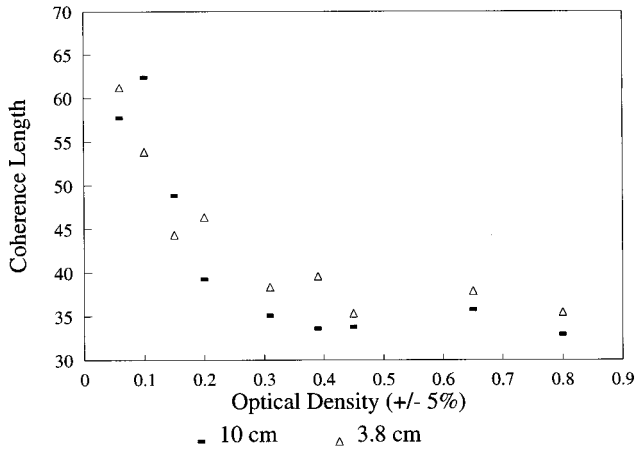

FIG. 7. Coherence length vs optical density for laser in water with diatomaceous earth added for two aperture sizes: 10 and 3.8 cm.

In an attempt to determine whether the size of the receiver aperture affects the spectral broadening, the experiment was repeated for two apertures. One aperture was 10 cm in diameter and the other aperture diameter was 3.8 cm. For the smaller aperture we placed a piece of black cardboard with a 3.8-cm hole in front of the collection lens. Results are shown in Fig. 7. While best-fit curves would place the large-aperture data below the small-aperture data, the two data sets are not significantly different. We expected a greater change in the coherence length for the large aperture because it allows more scattered light into the detector. The data confirm this, though the change is not as great as expected.

Another experiment was performed to determine whether the polarization states of the light influenced the broadening. The output from the laser is linearly polarized in the vertical sense. An optical isolator was used to transform the linearly polarized laser output to a circularly polarized beam. The coherence lengths for the two polarization states are graphed versus the OD in Fig. 8. The circularly polarized data have consistently smaller coherence lengths (more broadening) than the linearly polarized data. This is not surprising since the linearly polarized light is constrained to scatter in the

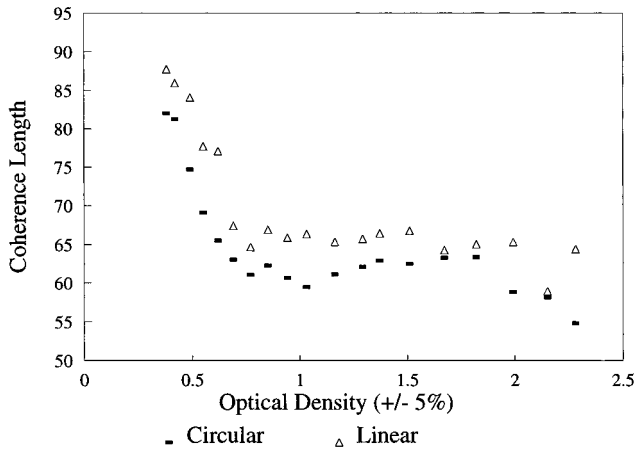

FIG. 8. Coherence length vs optical density for laser in water with 0.08-μm spheres added for circular and linear polarization states.

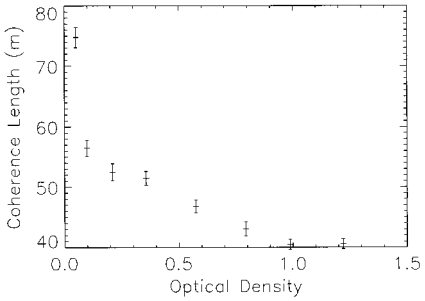

FIG. 9. Coherence length vs optical density for laser in water with 0.08-μm spheres added for the magnetic stirrers turned off.

plane perpendicular to the polarization. That is, the intensity distribution for plane-polarized Rayleigh scattering is proportional to $\cos^2\theta_s$. Vertically polarized light will not induce a dipole in the horizontal plane; therefore light will not be scattered in the vertical direction. Circularly polarized light can induce a dipole in any direction and therefore the small-angle scattering into the solid angle subtended by the detector is more uniform.

The magnetic stirrers were originally implemented to keep the diatomaceous earth in suspension. Since the density of diatomaceous earth is greater than that of water, it eventually settles on the bottom of the tank. The spheres have nearly the same density as water (1.055 g/cm^3), so they stay in suspension and the stirrers are (in principle) not needed. The stirrers set up currents and eddies, which may affect the broadening. In an effort to determine whether the stirrers affect the broadening, the experiment was repeated with the magnetic stirrers turned off. A consequence of turning the stirrers off was that the system had to be in equilibrium before measurements could be made. This took about 45 min per measurement (notice there are only a few data points). With the stirrers on, a homogeneous distribution of particles is attained very quickly after adding the spheres. Results are graphed in Fig. 9. Since the coherence length drops in the same manner as with the stirrers on, we conclude that the drop is not associated with macroscopic eddies and current flow.

A final experiment was performed with a dilute solution of spheres. The purpose was to more clearly define the l_c vs OD curve when the coherence length (spectral broadening) first starts to change. The polystyrene sphere solution was diluted and added one drop at a time as successive measurements were taken. The OD was not recorded for this experiment because the increments were too fine for the transmissometer to distinguish. Figure 10 is a graph of the coherence length versus density of spheres. The coherence length does not begin to decrease until nine drops have been added. By comparison to previous data, this corresponds roughly to $D_{\text{opt}}=0.16$. The average distance between spheres at this point is 9.3 μm. There were a total of 26 drops of diluted spheres added throughout the experiment, which roughly corresponds to an OD of 0.25. These data provide a finer analysis of the dependence of coherence length on density of spheres added.

If the distance between spheres is a significant parameter affecting l_c, then it is not surprising that larger spheres yield a null result. For the 0.08-μm spheres, the l_c begins to drop when the average distance between spheres is 9.3 μm. For

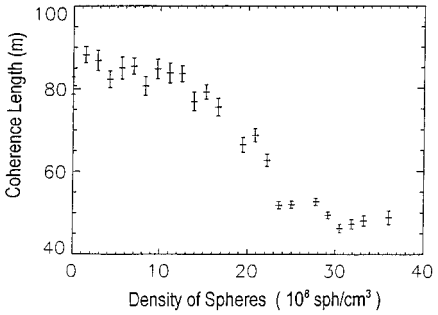

FIG. 10. Coherence length vs optical density for laser in water with diluted 0.08-μm spheres added.

the 5.17-μm spheres, the beam was extinguished (no signal from the detector) after the addition of 71 drops. This corresponds to an average distance between spheres of 338 μm. The beam was extinguished for the 0.54-μm spheres after 13 drops were added, corresponding to a mean distance between spheres of 74 μm. If the broadening is associated with the separations between the spheres becoming comparable to the wavelength of the light, then the separation of the larger spheres never reaches this length scale before the beam is completely attenuated.

The structure function given in Eq. (20) for the scattered spectrum is a sum of two Lorentzian spectra. Since we wish to compare our measured spectra against this structure function, we applied a curve fitting routine to our spectral data. The curve fitting routine compared the data with a numerically generated Voigt function. The composite Gaussian and Lorentzian width's were adjusted and updated until the best fit was found. The routine was applied to all data in the set for the polystyrene spheres in Figs. 3 and 4. The best-fit Gaussian and Lorentzian half-widths are graphed in Fig. 11. The Lorentzian width remains constant for all ODs, while the Gaussian width increases and levels off at about $D_{\mathrm{opt}} = 1$. This suggests that the broadening mechanism is governed by Gaussian rather than Lorentzian statistics. This is discussed further in the next section.

The plots of l_c versus OD in Figs. 4 and 6–8 have a slight

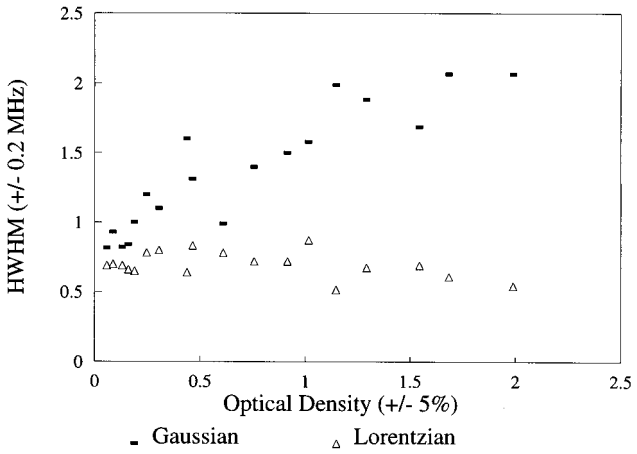

FIG. 11. Gaussian and Lorentzian half-widths vs optical density for 0.08-μm-sphere measurements.

rise at $D_{\mathrm{opt}} \approx 0.6$. This rise corresponds to a slight dip in the plots of the linewidth versus OD in Fig. 11. It was first thought that this was due to statistical fluctuations in the data; however this rise and dip showed up on every data run taken for diatomaceous earth and 0.08-μm spheres. Figure 12 shows plots of the curves of l_c versus OD for several data runs. The curves are offset to illustrate the slight rise in the data. This is not understood; we mention it only as a point of interest.

IV. COMPARISON OF THEORY TO EXPERIMENT

The theoretical spectral intensity distribution function in Eq. (15) was derived assuming monochromatic incident light. Since the bandwidth of the measured spectrum of the laser in air (the convolution of the laser spectrum and the instrumental response) is on the same order as the measured broadening, it cannot be considered a monochromatic source (a δ function). Since this ideal situation was not met in these experiments, we must convolve the theoretical scattered spectrum with the measured spectrum through clear water and compare to the measured spectrum through turbid water.

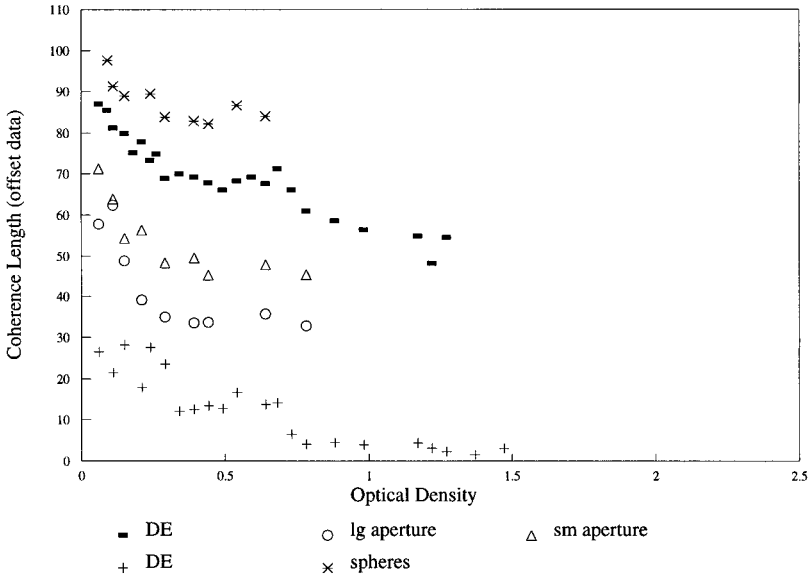

FIG. 12. Coherence length vs optical density offset curves. Each curve represents a separate data run. The value of the coherence length is offset to illustrate that each data run has a small peak at $D_{\mathrm{opt}} \sim 0.6$.

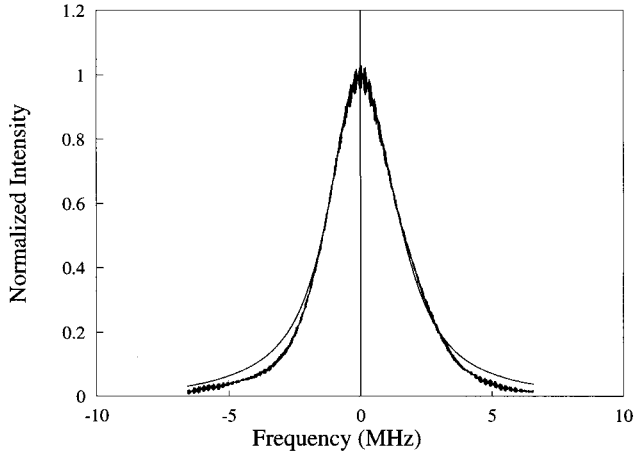

FIG. 13. Comparison of measured power spectrum with theoretical power spectrum for scattering from a binary fluid.

In calculating the structure function in Fig. 1 we assumed 50% scattering from particles and 50% scattering from thermal fluctuations. A more realistic situation would be 90–95 % scattering from particles and 5–10 % scattering from thermal fluctuations, as has been measured for other types of binary mixtures [22]. In an effort to determine the effect of the two types of scattered spectra on the structure function we varied the coefficients A and B in Eq. (19). The resulting spectra were convolved with the measured spectrum in clear water ($D_{\rm opt}=0.048$) for the 0.08-μm sphere data from Fig. 3. The resulting spectra for the various values of A and B were compared with each other and it was found that the convolved spectra were indistinguishable for $B=0.03-1.0$. Therefore, the width of the spectrum for scattering from the thermal fluctuations is so much greater than that for the particle diffusion component that the scattering from the thermal fluctuations need only be 3% or more for the measured spectrum to be dominated by scattering from the thermal fluctuations. This can be seen from Fig. 1, where the spectrum for scattering from the particles appears as a δ function with respect to the much broader (a few megahertz) spectrum for thermal scattering. Thus our data suggest that more than 3% of the scattering is from the thermal modes since scattering from particle diffusion would not have been resolvable with this detector. Even light multiply scattered from particle concentration fluctuations cannot give this much broadening. The maximum broadening for particle diffusion occurs when the scattering angle is 90°. The maximum change in the spectral width is therefore $Dq^2=D\{2k_0\ \sin(\theta)\}^2=3.2$ kHz. A photon shifted on the order of megahertz would have had to undergo ~300 scattering events, all additive at maximum scattering angle, and still enter the detector. Since the mean free path is never less than 0.5 m in our experiments and the length of the tank is 1.2 m, this cannot possibly be realized.

Assuming that the scattering from the thermal modes is 3% or greater, a curve was generated from Eq. (20), using only the thermal diffusion term. This was convolved with the measured spectrum taken through clear water ($D_{\rm opt}=0.048$) in Fig. 3. The results are plotted in Fig. 13 against the measured spectrum at $D_{\rm opt}=1.07$ from Fig. 3. The results are quite good around the peak and the widths are the same. Thus the thermal diffusion scattering gives the appropriate frequency shift. However, the measured spectrum diverges from the theoretical spectrum in the wings. This is because the spectrum in Eq. (20) is a Lorentzian distribution and the data have been shown to have a greater Gaussian component after broadening (Fig. 11). A characteristic of the Lorentzian is to taper off slowly, whereas the Gaussian tapers off more abruptly.

The measured spectrum at $D_{\rm opt}=1.07$ was chosen for comparison. The measured spectra and their associated coherence lengths do not change appreciably for optical densities greater than one. As discussed in Sec. II, at $D_{\rm opt}=1$ the mean free path is equal to the optical path length. The optical path length is the fixed length of the thank. Therefore, we postulate that for $D_{\rm opt}>1$ all of the collected light has scattered at least once. Multiple-scattering events occur for larger values of $D_{\rm opt}$, but those photons have a high probability of being scattered out of the beam. By choosing a scattered spectrum greater than but still close to $D_{\rm opt}=1$ we hope to satisfy the theoretical condition that all of the collected light has been single scattered.

V. DISCUSSION

The discrepancy between the theoretical spectrum and the measured spectrum seems to be because of the differences in the type of distribution functions. In this analysis we have assumed that (a) all the light collected after passing through clear water ($D_{\rm opt}=0.048$) has not been scattered, (b) all the light collected after passing through turbid water ($D_{\rm opt}=1.07$) has been scattered once, and (c) all the scattered light has been deflected through an angle $\theta=0.08$ rad. Even if conditions (a) and (b) are met, condition (c) is not. The angle $\theta=0.08$ rad was used because it is the maximum allowable angle, determined by the geometry of the experiment (Fig. 2), if the scattering event took place exactly in the middle of the tank. The frequency distribution of the scattered light is dependent, through the scattering vector q, on θ. The Rayleigh phase function for unpolarized (or circularly polarized) light is, $(3/16\pi)(1+\cos^2\theta)$. This can be considered the probability distribution for scattering at angle θ. Given θ, the probability that the scattered photon has a frequency between ω and $\omega+d\omega$ is

$$\frac{1}{\pi}\,S(k,\omega)\,d\omega=\frac{1}{\pi}\,\frac{\chi 4k_0^2\sin^2\dfrac{\theta}{2}}{\omega^2+\left(\chi 4k_0^2\sin^2\dfrac{\theta}{2}\right)^2}\,d\omega. \qquad (22)$$

Equation (22) is the thermal diffusion term from Eq. (20) with the scattering vector $q=2k_0\sin\theta/2$. Any given photon is scattered into an angle with a probability given by the Rayleigh phase function and constrained by the geometry of the experiment. Since the scattering volume is large, the maximum allowable angle is determined by the position in the tank where the scattering event took place. The scattered photon then has a given frequency with probability given by Eq. (22). Each photon may be scattered through a different angle with each angle having an associated frequency distribution. This process may introduce enough randomness for the overall frequency distribution to have a significant Gaussian character.

If each measured spectrum is a large random sample of the frequency of photons originating from events occurring throughout the scattering volume, then, by the central limit theorem, the measured frequency distribution will be Gaussian, regardless of the distributions of the individual events. The necessary conditions for the central limit theorem to hold are (i) the means of the distributions of the individual events are finite and (ii) the variances of the distributions of the individual events are positive definite. There exist three distinct random processes. The first process involves the number of photons that scatter at a point p in the tank. The next process describes the number of photons scattered at p into an angle θ, where θ is less than the maximum detectable angle. Finally, the last process, given by Eq. (22), determines the allowable frequencies for the photons scattered through an angle θ. In all three cases their respective means are finite and the variances are positive definite.

VI. CONCLUSION

An exhaustive study was undertaken to determine the cause of observed broadening in the spectrum of laser light scattered through water with colloidal particles added. It was found that the only mechanism, consistent with observation, that gives the correct order of magnitude for the spectral width is the coupled concentration-thermal fluctuations. In order to apply this theory we assumed the water-particle mixture can be described as a binary fluid mixture.

Though the concentration-thermal fluctuations give the appropriate energy shifts for the measured broadening, the spectral data diverge from the theory in the wings (Fig. 13). This is because the scattered spectrum for concentration-thermal fluctuations is Lorentzian, while the best fit to the data is a scattered spectrum with a larger Gaussian than Lorentzian component. Given the large scattering volume and the corresponding range of acceptance angles, we invoke the central limit theorem to explain why the measured spectra have a larger Gaussian component. This situation could be remedied by scattering from a small volume at a fixed, known angle. Then the scattered spectrum should have a greater Lorentzian component and give better agreement with the theoretical spectrum. A more difficult method of resolving the disparity between theory and experiment would be to simulate the scattering with a Monte Carlo model. If the distributions for each event (scattering position, angle, and frequency shift) are known, then a Monte Carlo simulation can be performed to obtain a resulting frequency distribution. This distribution could then be compared to the spectra measured through turbid water.

Spectral broadening was only observed for water-particle mixtures when the particles were smaller than the wavelength of the illuminating laser. There was no observed spectral broadening when larger spheres were added. The data for the dilute spheres, shown in Fig. 10, indicate that the spectrum is not significantly broadened until the ninth drop of spheres has been added. This corresponds to an average distance between particles of 9.3 μm. The larger spheres never approach this separation distance before the beam is extinguished. We postulate that the average distance between particles must be small enough before the concentration gradients of the particles interact significantly with the thermal fluctuations.

ACKNOWLEDGMENT

This work was supported under the internal Independent Research program, funded by the Office of Naval Research, at the Coastal Systems Station.

[1] See, for example, R. Crane, Opt. Eng. **18**, 205 (1979).
[2] P. A. Fleury and J. P. Boon, *Advances in Chemical Physics* (Wiley, New York, 1973), Vol. 24, pp. 9–13.
[3] P. A. Fleury, *Physical Acoustics* (Academic, New York, 1970), Vol. 6, pp. 9–13.
[4] D. McIntyre and J. V. Sengers, *Physics of Simple Liquids* (North-Holland, Amsterdam, 1968), pp. 475–486.
[5] H. Z. Cummins and R. W. Gammon, J. Chem. Phys. **44**, 2785 (1966).
[6] D. H. Rank, E. M. Kiess, U. Fink, and T. A. Wiggins, J. Opt. Soc. Am. **55**, 925 (1965).
[7] R. Pecora, J. Chem. Phys. **40**, 1604 (1964).
[8] R. D. Mountain, Rev. Mod. Phys. **38**, 205 (1966).
[9] B. J. Berne and R. Pecora, *Dynamic Light Scattering* (Wiley, New York, 1976), pp. 233–254.
[10] R. Schmitz, Physica A **206**, 25 (1994).
[11] W. B. Li, P. N. Segre, R. W. Gammon, and J. V. Sengers, Physica A **204**, 399 (1994).
[12] J. W. Goodman, *Statistical Optics* (Wiley, New York, 1985), p. 167.
[13] W. H. Flygare, *Molecular Structure and Dynamics* (Prentice-Hall, Englewood Cliffs, NJ, 1978), Chap. 1.
[14] See, for example, J. D. Jackson, *Classical Electrodynamics* (Wiley, New York, 1975), p. 393.
[15] See, for example, R. Loudon, *The Quantum Theory of Light*, 2nd ed. (Oxford University Press, Oxford, 1983), pp. 292–295.
[16] R. D. Mountain and J. M. Deutch, J. Chem. Phys. **50**, 1103 (1969).
[17] S. R. de Groot and P. Mazur, *Non-Equilibrium Thermodynamics* (North-Holland, Amsterdam, 1962), p. 278.
[18] The Fabry-Pérot spectrometer was a Coherent model 216-A. The appearance of trade names in this document does not constitute endorsement by the Department of Defense; the Navy; or the Coastal Systems Station Dahlgren Division, Naval Surface Warfare Center.
[19] R. Pecora and W. A. Steele, J. Chem. Phys. **42**, 1872 (1965).
[20] D. A. Pinnow, S. J. Candau, and T. A. Litovitz, J. Chem. Phys. **49**, 347 (1968).
[21] A. Corney, *Atomic and Laser Spectroscopy* (Clarendon, Oxford, 1977), p. 260.
[22] M. F. Vuks, Opt. Spectrosc. **28**, 71 (1970).
[23] *CRC Handbook of Chemistry and Physics*, edited by R. C. Weast (CRC Press, Boca Raton, FL, 1974).